

Infrared microthermometric and stable isotopic study of fluid inclusions in wolframite at the Xihuashan tungsten deposit, Jiangxi province, China

Wenfeng Wei · Ruizhong Hu · Xianwu Bi ·
Jiantang Peng · Wenchao Su · Shengqiong Song ·
Shaohua Shi

Received: 29 September 2010 / Accepted: 30 June 2011 / Published online: 30 July 2011
© Springer-Verlag 2011

Abstract The Xihuashan tungsten deposit, Jiangxi province, China, is a world-class vein-type ore deposit hosted in Cambrian strata and Mesozoic granitic intrusions. There are two major sets of subparallel ore-bearing quartz veins. The ore mineral assemblage includes wolframite and molybdenite, with minor amounts of arsenopyrite, chalcopyrite, and pyrite. There are only two-phase aqueous-rich inclusions in wolframite but at least three major types of inclusions in quartz: two- or three-phase CO₂-rich inclusions, two-phase pure CO₂ inclusions and two-phase aqueous inclusions, indicating boiling. Fluid inclusions in wolframite have relatively higher homogenization temperatures and salinities (239–380°C, 3.8–13.7 wt.% NaCl equiv) compared with those in quartz (177–329°C, 0.9–8.1 wt.% NaCl equiv). These distinct differences suggest that those conventional microthermometric data from quartz are not adequate to explain the ore formation process. Enthalpy–salinity plot shows a linear relationship, implying mixing of different sources of fluids. Although boiling occurred during vein-type mineralization, it seems negligible for wolframite deposition. Mixing is the dominant mechanism of wolframite precipitation in Xihuashan. $\delta^{34}\text{S}$ values of the sulfides range from –1.6 to +0.1‰, indicative of a magmatic source of sulfur. $\delta^{18}\text{O}$ values of wolframite are

relatively homogeneous, ranging from +4.8‰ to +6.3‰. Oxygen isotope modeling of boiling and mixing processes also indicates that mixing of two different fluids was an important mechanism in the precipitation of wolframite.

Keywords Infrared microthermometry · Fluid inclusions · Tungsten deposit · Stable isotopes · Xihuashan · China

Introduction

Granite-associated tungsten deposits are well-known in the literature (Higgins 1985; Polya et al. 2000; Rice et al. 2001; Lu et al. 2003; Rios et al. 2003; Burnard and Polya 2004; Petrunic and Al 2005; Macey and Harris 2006; Gu et al. 2007), but the mechanism of ore deposition is still a matter of debate. Mechanisms that initiate the precipitation of wolframite include pressure decrease (Polya 1989), cooling (Heinrich 1990; Samson 1990; Xi et al. 2008), wall-rock alteration (Gong et al. 2004), boiling (So and Yun 1994; Graupner et al. 1999), and fluid mixing (Yokart et al. 2003; Beuchat et al. 2004). Among these, boiling and mixing of magmatic and meteoric waters are thought to be significant in the formation of the unconventionally high ore grades of some tungsten deposits (Landis and Rye 1974; Kelly and Rye 1979). However, the importance of boiling or mixing is not well examined in this type of mineralization.

China ranks first in the world in terms of tungsten resources and reserves (USGS 2010). The Xihuashan tungsten deposit is famous throughout the world for its large-scale and long history of geological exploration and investigation. It is an ideal place to study the above-mentioned issues of tungsten mineralization. Previously, fluid inclusion-oriented studies on this deposit were

Editorial handling: B. Lehmann

W. Wei · R. Hu (✉) · X. Bi · J. Peng · W. Su · S. Song · S. Shi
State Key Laboratory of Ore Deposit Geochemistry,
Institute of Geochemistry, Chinese Academy of Sciences,
Guiyang 550002, China
e-mail: huruizhong@vip.gyig.ac.cn

W. Wei · S. Song · S. Shi
Graduate University of Chinese Academy of Sciences,
Beijing 100049, China

confined to transparent gangue minerals (Sheng 1985; Lu 1986; Giuliani et al. 1988; Liu et al. 2002) because most ore minerals are opaque under the normal petrographic microscope. However, fluid inclusions trapped in gangue minerals are not necessarily representative of the actual conditions under which the ore minerals were precipitated (Campbell et al. 1984; Campbell and Panter 1990; Lüders 1996). Thus, direct analysis of fluid inclusions in ore minerals is required. Infrared microscopy is approved to be useful for examining fluid inclusions in opaque minerals (Richards and Kerrich 1993; Lüders et al. 1999, 2005, 2009; Lüders and Ziemann 1999; Lindaas et al. 2002; Kouzmanov et al. 2004; Rosiere and Rios 2004; Ni et al. 2008; Cao et al. 2009; Kucha and Raith 2009). In particular, infrared microscopy technology is widely used in the study of fluid inclusions in wolframite (Campbell and Panter 1990; Lüders 1996; Bailly et al. 2002; Rios et al. 2006). In this paper, we use this technique to examine fluid inclusions in wolframite from the Xihuashan deposit.

The objectives are to obtain information directly on the mineralizing fluids and to gain further insight into the evolution of fluids. New infrared investigation data from the fluid inclusions in wolframite are obtained and reported. In addition, stable isotope (S, O) data of ore minerals are used to evaluate the source of the ore-forming fluids and the mechanism of ore deposition. Although boiling occurs during mineralization, fluid mixing is proved as the dominant precipitation mechanism for wolframite.

Regional geological setting

South China is composed of the Yangtze Block to the northwest and the Cathaysian Block to the southeast, separated by the Jiangshan-Shaoxing fault (Fig. 1). The two blocks were welded during Neoproterozoic time (Zhou et al. 2002; Yan et al. 2003). The Yangtze Block, separated from the North China Block by the Qinling-Dabie orogenic belt to the north, is bounded to the west by the Tibetan Plateau. The Cathaysian Block has a Precambrian basement overlain by a Sinian to Mesozoic cover sequence (Chen and Jahn 1998). The Xihuashan tungsten deposit is located in the western Cathaysian Block (Fig. 1).

In South China, extensive magmatism produced Mesozoic granitoid intrusions (Li et al. 2009). Metallic mineralization in the Cathaysian block was associated with the widespread Jurassic to Cretaceous (Yanshanian) granitic magmatism (Hsieh et al. 2008). The granites are traditionally thought to be S-type or transitional type (Mo et al. 1980), but they are also argued as A-type granites recently (Fan and Chen 2000; Wu et al. 2007; Hu et al. 2008; Li et al. 2009). Spatially, the distribution of the granitoid rocks is controlled by Mesozoic NE-striking faults (Peng et al. 2006).

South China is rich in mineral resources and especially renowned as the world's major tungsten-producer. There are various types of tungsten mineralization, i.e., greisen-, skarn-, altered granite-, and quartz vein-type, among which the quartz vein-type is the most important one. Temporally, these tungsten deposits are related to Yanshanian granites and coincident with crustal extension (Mao et al. 2007).

Geology of the Xihuashan ore deposit

The Xihuashan deposit is a typical vein-type tungsten polymetallic deposit and occurs in the endocontact zones of a Yanshanian composite granitic stock (Wu et al. 1987; Chang et al. 2007; Zhou et al. 2008). This deposit, together with five surrounding much smaller deposits constitutes a tungsten ore field (Fig. 2). In the Xihuashan mining district, exposed sedimentary rocks are mainly early Paleozoic (upper Cambrian) metasediments and slate intruded by Jurassic and Cretaceous (Yanshanian) granite (Fig. 2). The Cambrian strata underwent low-grade metamorphism. The petrology of the complex was described by many geologists (Le Bel et al. 1984; Giuliani 1985; McKee et al. 1987; Wu et al. 1987; Maruéjol et al. 1990; Zeng et al. 2001; Wang et al. 2003). Spatially, this granitic complex is distributed along EW- or NNE- orientated structures (Wu et al. 1987; Xie et al. 2008). It is a polyphase intrusion composed of porphyritic biotite granites with coarse-grained, medium-grained, and medium- to fine-grained variants (Wang et al. 2003). The granite is strongly peraluminous, belonging to the high calc-alkaline series and is usually considered as S-type granite (Wu et al. 1987; Shen et al. 1994; Zeng et al. 2001; Xiao et al. 2009). The ore veins are spatially and genetically associated with this granite (Tanelli 1982; Giuliani 1985; Chang et al. 2007; Zaw et al. 2007).

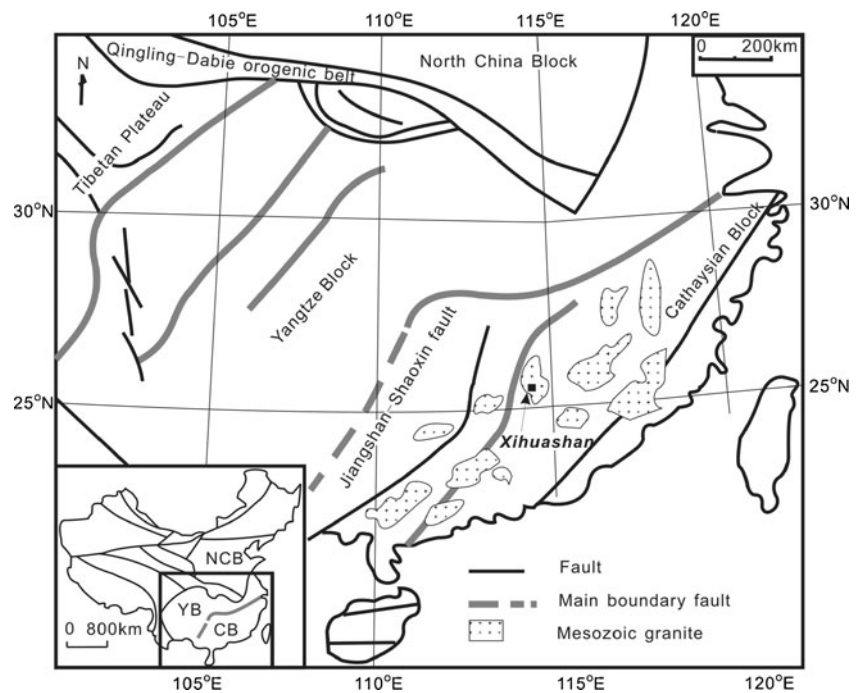
Nature of the ore veins

There are more than 700 ore veins in the Xihuashan mining district. In general, the veins vary from 200 to 600 m in length and about 0.2 to 0.6 m in thickness. These veins can be divided into two sets according to their orientation and location. In the northern part of the mining area, they dip steeply (75–85°) with an EW strike. However, they dip more steeply (80–85°) and strike ENE in the south. These veins usually show an echelon structure and are distributed in groups or clusters (Giuliani et al. 1988). The total resource is 81,300 tonnes WO₃, with an average ore grade of 1.08% WO₃.

Mineralogy and paragenesis

The mineralogy and paragenesis of the Xihuashan deposit have been documented previously (Tanelli 1982; Lu 1986;

Fig. 1 A geological sketch map of South China showing the main tectonic blocks and the location of the Xihuashan tungsten deposit (modified from Yan et al. 2003). *YB* Yangtze block, *CB* Cathaysian block, *NCB* North China block



Wu et al. 1987; Giuliani et al. 1988). Based on mineral assemblages, crosscutting relationships and textures, the paragenetic sequence of the mineralized quartz veins consists of an early silicate-oxide stage, followed by a sulfide stage, and a later carbonate stage (Tanelli 1982; Lu 1986; Wu et al. 1987; Giuliani et al. 1988; Chang et al. 2007). Features of each stage are summarized in Fig. 3.

The silicate-oxide stage consists mainly of massive quartz with wolframite, molybdenite, beryl, feldspar (Fig. 4a, d). Quartz, the most abundant mineral, appears mainly anhedral but is also found as prismatic crystals in vugs (Wu et al. 1987). As the most abundant ore mineral, wolframite occurs mainly as euhedral, dark-brown masses. Euhedral wolframite is mainly found attached to the vein walls, with a central filling of massive quartz, and is seldom found embedded in the massive quartz (Fig. 4b; Tanelli 1982; Lu 1986; Wu et al. 1987). In some cases, wolframite is disseminated in the host granite (Fig. 4e). It can be concluded that quartz is younger than wolframite, and wolframite preceded quartz with some depositional overlap (Lu 1986; Lu et al. 2003). The earliest mineral in the hydrothermal veins is feldspar (Fig. 3). Molybdenite, the earliest sulfide, occurs as euhedral or anhedral masses at vein margins or intergrown with chalcopyrite near vein centers, and arsenopyrite occurs as euhedral or anhedral masses that are associated with wolframite (Wu et al. 1987). Generally, pyrite is intergrown with chalcopyrite near vein centers or in the microfractures in wolframite (Fig. 4f).

The sulfide stage is characterized by the presence of pyrite, arsenopyrite, chalcopyrite, sphalerite, galena, and quartz (Fig. 4c, g–i), with trace amounts of wolframite. In addition,

pyrrhotite and bismuthinite have also been observed (Giuliani et al. 1988; Xie et al. 2009). Euhedral or subhedral pyrite, the most abundant sulfide, is generally associated with arsenopyrite, chalcopyrite-diseased sphalerite, and chalcopyrite or occasionally enclosed in chalcopyrite (Fig. 4g–i).

The carbonate stage is marked by the appearance of calcite and quartz with trace amounts of pyrite and chalcopyrite but no wolframite (Lu 1986; Giuliani et al. 1988).

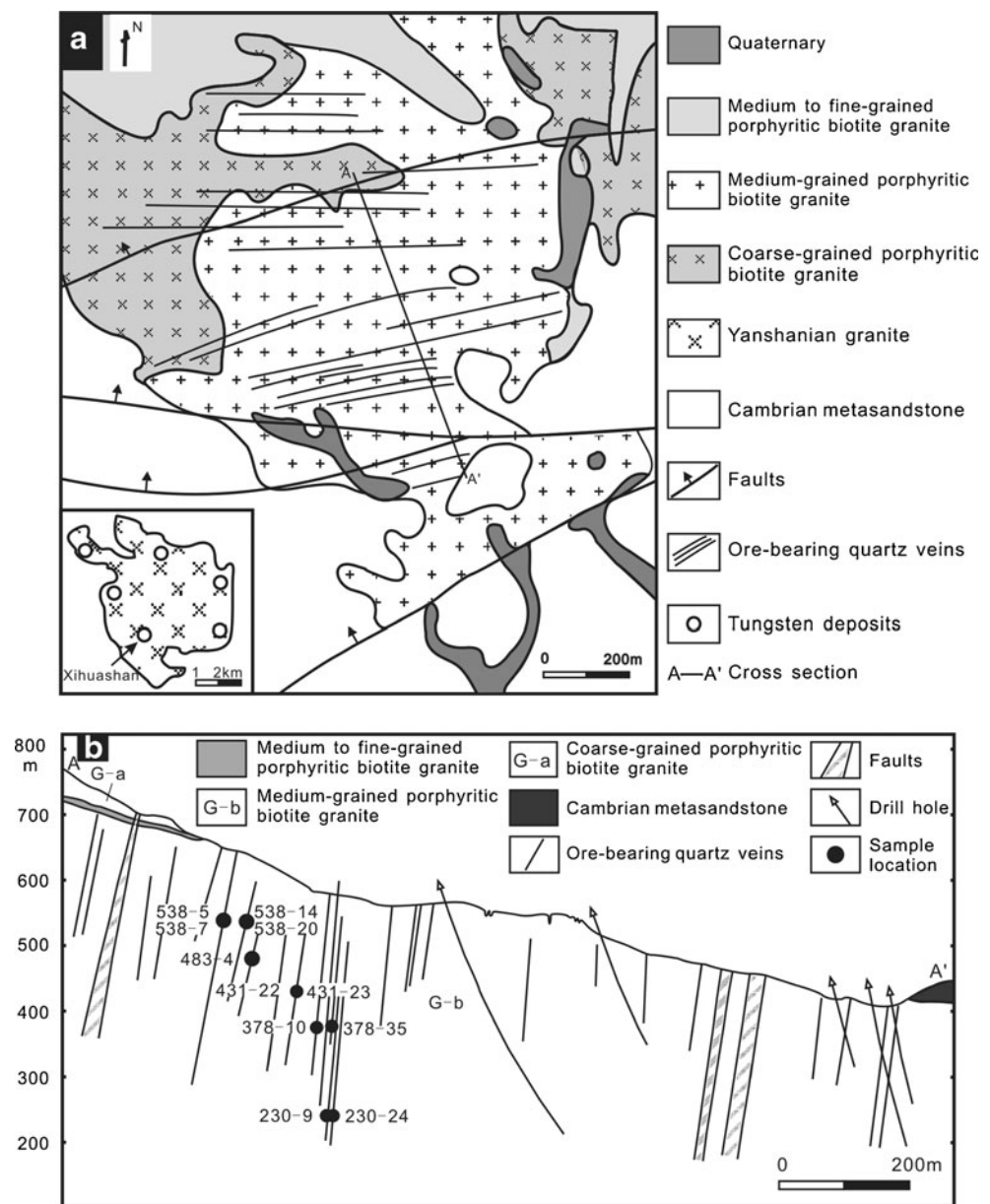
Samples and analytical methods

Fluid inclusions

Fluid inclusions were examined in both wolframite and quartz from the silicate-oxide and sulfide stages (Fig. 2b). The thickness of doubly polished sections of wolframite was about 90 to 120 μm and about 200 μm for quartz.

The microthermometric study of fluid inclusions trapped in wolframite was performed using a heating–freezing system mounted on an Olympus BH51 infrared microscope at the State Key Laboratory of Ore Deposit Geochemistry, Institute of Geochemistry, Chinese Academy of Sciences, Guiyang, China. Temperatures of phase changes are influenced by the infrared light source intensity, and therefore it is necessary to turn off all possible diaphragms to minimize this analytical error (Moritz 2006). Because ice is not observed in some inclusions and thick inclusion borders often obscure the vapor phase during the approach to homogenization (Mancano and Campbell 1995), T_m and T_h values were measured using a cycling method described by Goldstein

Fig. 2 Geological map of the Xihuashan tungsten deposit (a; modified from Wu et al. 1987) and cross-section with sample location (b)



and Reynolds (1994). Quartz-hosted fluid inclusions were measured by conventional microthermometry using a Linkam THMSG 600 stage, calibrated at -56.6°C , 0°C , and 374.1°C using synthetic fluid inclusions. The precisions of the measurements are $\pm 0.2^{\circ}\text{C}$ and $\pm 2^{\circ}\text{C}$ in cooling cycles and heating cycles, respectively. Temperatures of phase transitions were observed at a heating rate of $0.1^{\circ}\text{C}/\text{min}$. Laser Micro-Raman spectroscopic analysis was carried out on a Renishaw InVia Reflex Raman spectrometer with the counting time of 60 s.

Salinity and density of liquid-vapor inclusions were estimated by using the online calculation of Duan (www.geochem-model.org). Salinities of CO_2 -rich inclusions were calculated from the melting temperature of clathrate. Bulk composition and molar volume were determined with the

computer programs of Brown (1989) and the equation of state from Duan et al. (1995).

Stable isotopes

Representative samples from the Xihuashan deposit were chosen for picking mineral separates for sulfur and oxygen isotope analyses. Wolframite and sulfide minerals, pyrite, arsenopyrite, chalcopyrite, and molybdenite were separated by careful handpicking under a binocular microscope.

Oxygen isotope compositions of wolframite separates were measured at the Laboratory of Stable Isotope Geochemistry, Institute of Mineral Resources, Chinese Academy of Geological Sciences, Beijing, using a MAT 253 mass spectrometer. Oxygen isotopes were analyzed with the conventional BrF_5

Mineral \ Stage	Silicate-oxide	Sulfide	Carbonate
Feldspar	————		
Muscovite	————		
Cassiterite	-----		
Topaz	-----		
Beryl	-----		
Molybdenite	-----	-----	
Wolframite	————	————	
Quartz	-----		-----
Fluorite	-----	-----	-----
Scheelite	-----	-----	
Helvite	-----	————	
Arsenopyrite	-----	————	
Pyrite	-----	-----	-----
Pyrrhotite		-----	
Sphalerite		————	
Chalcopyrite		-----	
Galena		————	
Bismuthinite		————	
Dolomite			————
Calcite			————

Fig. 3 Paragenetic sequence of minerals from the Xihuashan tungsten deposit

method (Clayton and Mayeda 1963). All values are reported relative to the V-SMOW standard, with the error of $\pm 0.2\%$.

Sulfur isotope analyses were performed at the State Key Laboratory of Environmental Geochemistry, Institute of Geochemistry, Chinese Academy of Sciences, Guiyang, China, by using the continuous flow isotope ratio mass spectrometry. The procedures described by Grassineau et al. (2001) were followed during the analysis. The data are reported relative to CDT, and the analytical precision is $\pm 0.2\%$.

Fluid inclusions

Petrography

Fluid inclusion analysis in wolframite and quartz is focused on fluid inclusion assemblages if the inclusions were trapped along growth zones or healed microfractures (Goldstein and Reynolds 1994; Lüders et al. 2009). At Xihuashan, the lack of growth banding in quartz makes it difficult to classify fluid inclusions based on above criteria. In this study, fluid inclusion data of quartz were obtained from some isolated inclusions that might be primary in origin according to Roedder (1984) or groups of inclusions that have similar vapor-to-liquid ratios, as well as heating and freezing behavior. Such fluid inclusion assemblages can provide the most reliable information (Rusk et al. 2008).

Wolframite

Apparent growth banding is observed in wolframite (Fig. 5a). In some cases, fluid inclusions are arranged along or within

the growth banding. Microscopic and microthermometric observations displayed two-phase liquid-rich aqueous inclusions at an ambient temperature. Two- or three-phase CO_2 -rich or vapor-rich inclusions are not observed in wolframite. Tubular shaped or subrounded inclusions (Fig. 5b–f) range from a few microns to more than 20 μm . The vapor phase is approximately 8–30% of the total volume of the inclusion. Primary inclusions often occur within the growth banding (Fig. 5b–d), and some isolated inclusions (Fig. 5e, f) also can be of primary origin (Roedder 1984; Lüders et al. 2009).

Quartz

At Xihuashan, fluid inclusions in quartz include types I, II, and III, on the basis of their appearance at 25°C and by their Raman spectra. Type I inclusions are two-phase, liquid-rich aqueous inclusions. The most abundant inclusions of quartz from the silicate-oxide and sulfide stages are type I. They occur both as individual isolation or groups (Fig. 5g, h), with 10 to 30 vol.% at room temperature, ranging from 5 to 35 μm in diameter. These inclusions have typically rounded rectangles and ellipsoids. Both microthermometry and Raman spectroscopy analyses reveal that the main component of the volatile phases is H_2O , with minor CO_2 and trace CH_4 in some cases.

Type II inclusions are two-phase CO_2 -rich inclusions (aqueous solution + CO_2 vapor, type IIa) or three-phase CO_2 -rich inclusions (aqueous solution + liquid CO_2 + CO_2 vapor, type IIb) at room temperature. They are observed only in quartz from the silicate-oxide stage and occur isolated or in groups together with liquid-rich aqueous inclusions or pure CO_2 inclusions (Fig. 4i–l). Type II inclusions are typically 8–35 μm in diameter and have nearly ellipsoidal, rounded-rectangular, or irregular shapes. The CO_2 phase typically occupies 25% to 90% of the inclusion volumes. Both microthermometry and Raman spectroscopy analyses reveal that the main component of the volatile phase is CO_2 .

Type III inclusions are relatively rare and are two-phase pure CO_2 inclusions (liquid CO_2 + CO_2 vapor). They are generally less than 15 μm in diameter and are observed in quartz from the silicate-oxide stage. They can coexist with three-phase CO_2 -rich inclusions and liquid-rich aqueous inclusions (Fig. 4j).

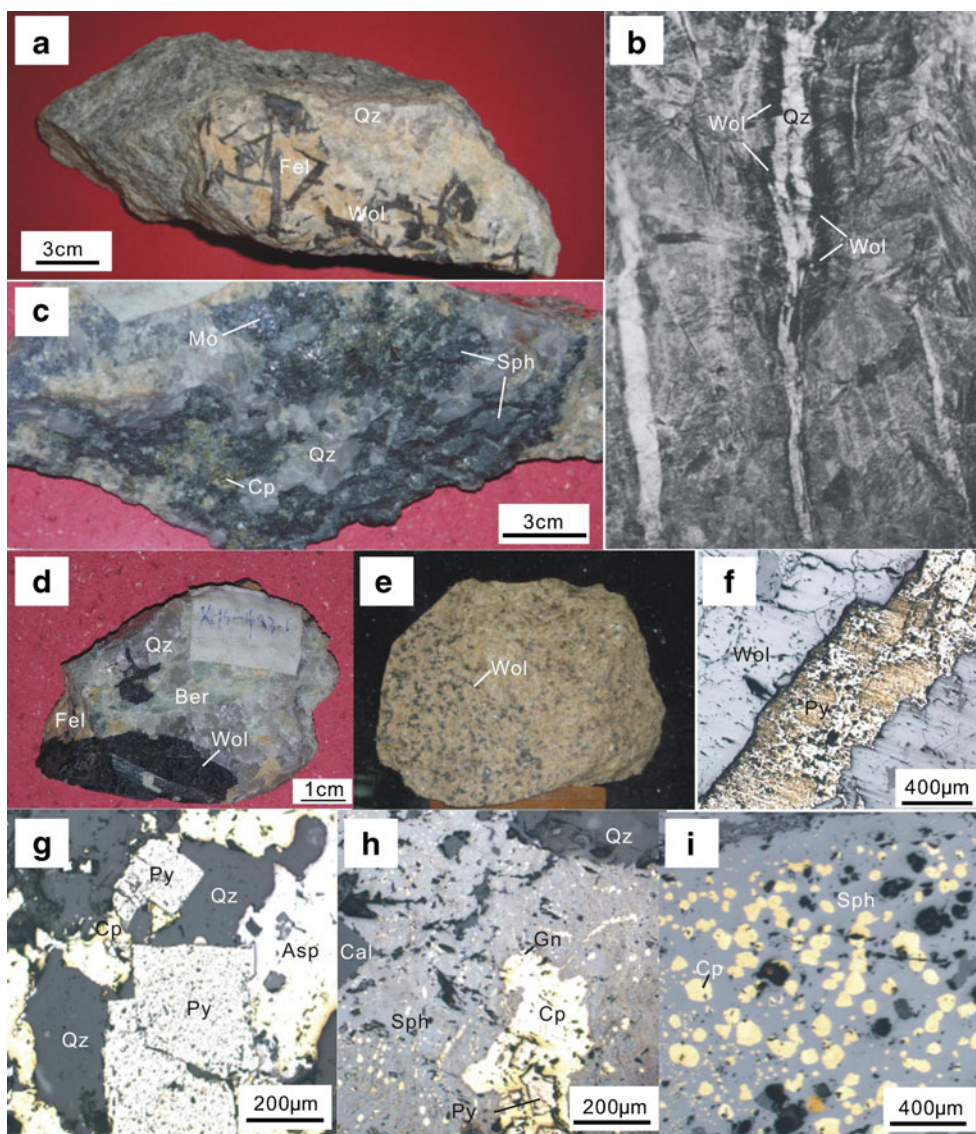
Microthermometric results

Microthermometric results of fluid inclusions in wolframite and quartz are summarized in Table 1.

Wolframite

Final ice melting temperatures of primary aqueous inclusions range from -2.1°C to -9.8°C , corresponding to salinities from

Fig. 4 Photographs (a–e) and photomicrographs (f–i) of ore and gangue minerals. **a, d** Ore minerals of the silicate-oxide stage. **b** Euhedral wolframite attached to the vein walls, with central infill of massive quartz (Tanelli 1982). **c** Ore minerals of the sulfide stage. **e** Disseminated wolframite in greisenized granite (photograph taken in Xihuashan museum.). **f** Pryrite infill in wolframite veinlet. **g** Pyrite intergrown with chalcopyrite and arsenopyrite of the sulfide stage. **h** Pyrite enclosed in chalcopyrite, and intergrown with galena, chalcopyrite-diseased sphalerite of the sulfide stage. **i** Chalcopyrite disease in sphalerite of the sulfide stage. *Wol* wolframite, *Fel* feldspar, *Ber* beryl, *Qz* quartz, *Py* pyrite, *Cp* chalcopyrite, *Asp* arsenopyrite, *Cal* calcite, *Sph* sphalerite, *Gn* galena



3.8 to 13.7 wt.% NaCl equiv, with an average of 6.8 wt.% NaCl equiv (Fig. 6a, Table 1). The relatively low salinity aqueous inclusions usually occur clustered together with relatively high salinity aqueous inclusions. Temperatures of homogenization to liquid phase for all fluid inclusions vary from 239°C to 380°C, mostly between 320°C and 370°C (Fig. 6b). The densities lie between 0.63 and 0.88 g/cm³.

Quartz

Type I liquid-rich aqueous inclusions have ice-melting temperatures (T_m) from -0.5°C to -5.2°C , corresponding to salinities of 0.9 to 8.1 wt.% NaCl equiv (Fig. 6c, Table 1), with an average of 4.2 wt.% NaCl equiv. Temperatures of homogenization to the liquid phase of these fluid inclusions range from 236°C to 325°C for the silicate-oxide stage and 177°C to 241°C for the sulfide stage (Fig. 6d). The densities vary from 0.74 to 0.90 g/cm³.

Type II inclusions form solid CO₂ upon cooling from -92.1°C to -97.6°C . Melting temperatures of the CO₂ phase range from -55.7°C to -57.2°C with a majority at -56.6°C (type IIa, -56.3°C to -57.1°C ; type IIb, -55.7°C to -57.2°C), indicative of a volatile phase of nearly pure CO₂, as further confirmed by laser Raman spectroscopy. The CO₂

Fig. 5 **a** Growth banding in wolframite. **b–l** Photomicrographs of representative fluid inclusion types in wolframite and quartz: **b–d** Primary liquid-rich aqueous inclusions within growth banding in wolframite. **e, f** Isolated aqueous inclusions in wolframite. **g** Isolated liquid-rich aqueous inclusion (type I) in quartz. **h** A group of liquid-rich aqueous inclusions in quartz. **i–k** Type I, type II and type III inclusions in one field of view in quartz, homogenization both to the vapor and liquid at about the same temperatures, indicative of boiling. **i** CO₂ of type IIa inclusion homogenizing to vapor phase at 28.7°C. **j** CO₂ of type IIb and type III inclusions homogenizing to liquid phase at 27°C and 30.7°C, respectively. **k** CO₂ of type IIb inclusion critical homogenization at 30.7°C. **l** CO₂ of type IIb inclusion in quartz homogenizing to vapor phase at 29°C

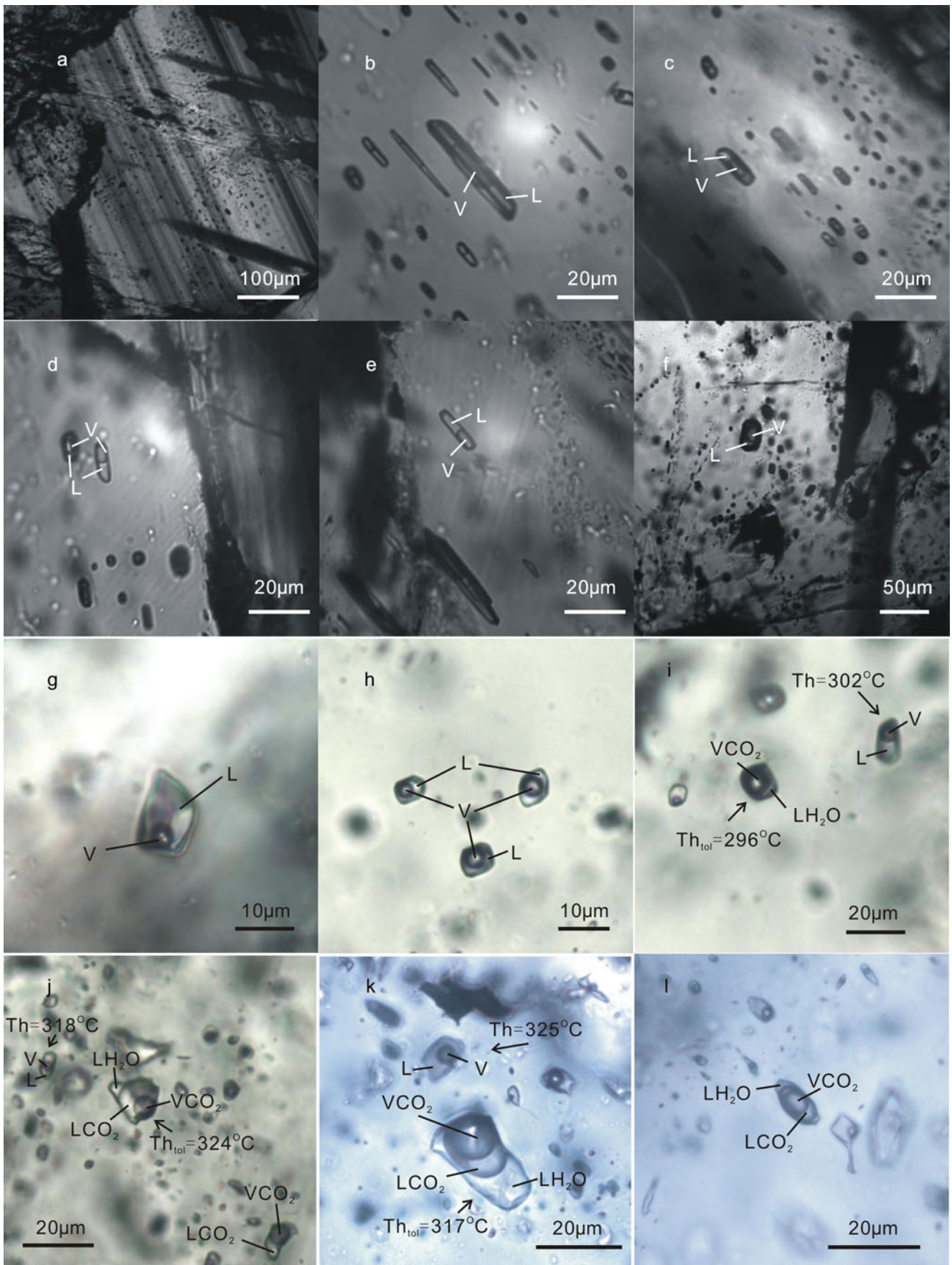


Table 1 Microthermometric data in the Xihuashan tungsten deposit, southern Jiangxi

Sample	Mineral	Type	Tm-CO ₂ (°C) ^a	Th-CO ₂ (°C) ^b	Th-CO ₂ (°C) ^c	Th-CO ₂ (°C) ^d	Tm-clathrate or Tm-ice (°C) ^e	Salinity	Th or Th-tot (V)(°C) ^f	Th-tot(L)(°C) ^g
Silicate-oxide stage										
378-35	Wolframite	I					-2.4 to -9.3 (19)	4.0–13.2 (19)	356–380 (28)	
431-22	Wolframite	I					-2.9 to -5.9 (17)	4.8–9.1 (17)	319–343 (33)	
431-23	Wolframite	I					-2.5 to -9.0 (10)	4.2–9.1 (10)	296–319 (19)	
483-4	Wolframite	I					-2.1 to -4.0 (7)	3.8–6.7 (7)	239–286 (6)	
538-7	Wolframite	I					-2.5 to -9.8 (16)	4.2–13.7 (16)	331–361 (27)	
538-20	Wolframite	I					-2.7 to -5.8 (12)	4.5–8.9 (12)	336–358 (28)	
378-10	Quartz	I					-3.0 to -5.2 (4)	5.0–8.1 (4)	290–316 (23)	
431-22	Quartz	I					-2.1 to -4.5 (24)	3.5–7.2 (24)	267–287 (44)	
431-23	Quartz	I					-2.4 to -3.2 (6)	4.0–5.3 (6)	241–259 (9)	
483-4	Quartz	I					-1.8 to -3.2 (13)	3.1–5.3 (13)	236–258 (27)	
538-5	Quartz	I					-2.1 to -3.6 (6)	3.5–5.9 (6)	284–320 (19)	
		IIb	-55.9 to -56.9 (15)	27.0–29.4 (7)	28.3–29.5 (6)	30.8 (2)	7.0–9.4 (15)	1.2–5.8 (15)	305–324 (5)	287–319 (8)
		III	-56.6 (1)	30.7 (1)						
538-14	Quartz	I					-1.7 to -2.8 (23)	5.0–6.2 (23)	278–325 (47)	
		IIa	-56.3 to -57.1 (4)	27.6–29.1 (4)			8.1–9.4 (4)	1.2–3.7 (4)	296 (1)	
		IIb	-55.7 to -57.2 (15)	27.5–28.9 (2)	26.9–30.7 (12)	30.7 (1)	7.9–9.2 (15)	1.6–4.1 (15)	303–329 (5)	289–317 (6)
		III	-56.6 (1)	30.6 (1)						
Sulfide stage										
230-9	Quartz	I					-1.1 to -3.1 (12)	1.6–5.1 (12)	193–241 (25)	
230-24	Quartz	I					-0.5 to -2.3 (19)	0.9–3.9 (19)	177–222 (26)	

Numbers in parentheses is the number of measurements. Salinity is in wt.% NaCl equiv

^a Final melting temperature of CO₂ in type II and III inclusions

^b CO₂ in type IIa, IIb, and III inclusions homogenization to liquid

^c CO₂ in type IIb inclusions homogenization to vapor

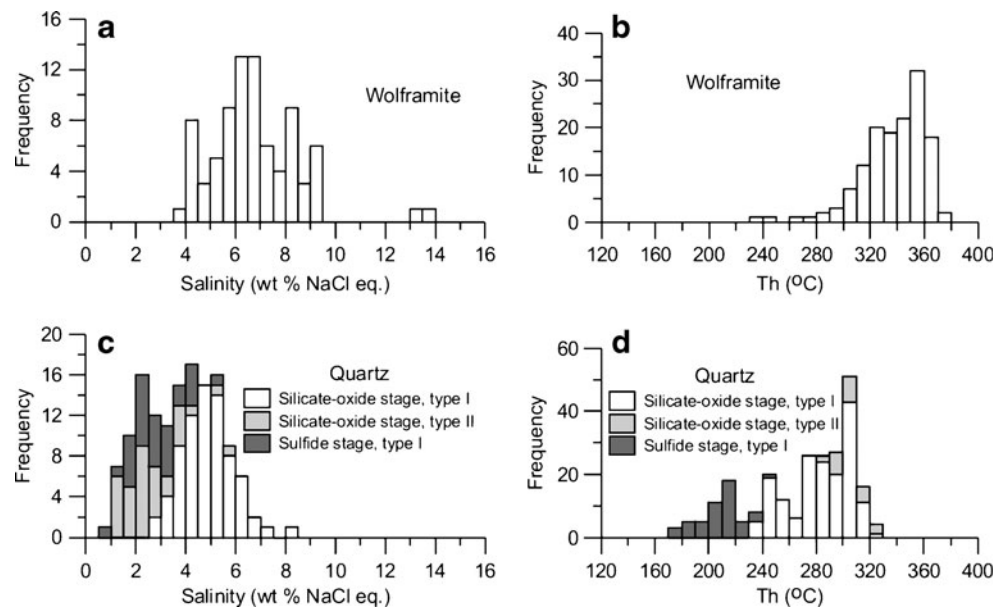
^d CO₂ in type IIb inclusions critical homogenization

^e Final melting temperature of ice in type I inclusions or final melting temperature of CO₂ clathrate in type II and III inclusions

^f Homogenization temperature of type I inclusions or total homogenization temperature of type IIa and IIb inclusions homogenized to CO₂ phase

^g Total homogenization temperature of type IIb inclusions homogenized to aqueous phase

Fig. 6 Histograms of homogenization temperatures and salinities of fluid inclusions in wolframite and quartz from Xihuashan



phase homogenizes to vapor from 27.6°C to 29.1°C for type IIa inclusions (e.g., Fig. 4i). However, the CO₂ phase homogenizes to liquid, to vapor, and by critical behavior (e.g., Fig. 4j–i) between 26.9°C and 30.8°C for type IIb inclusions (Fig. 7a). Clathrate melting temperatures of type II inclusions range from 7.0°C to 9.4°C, corresponding to salinities of 1.2 to 5.8 wt.% NaCl equiv. The density of the volatile phase lies between 0.23 and 0.68 g/cm³. Although some of the type II inclusions decrepitated before total homogenization on account of high internal pressures generated by their high CO₂ contents, the final homogenization temperatures of many type II inclusions could still be measured. Type II inclusions mostly homogenized to the aqueous phase from 287°C to 319°C, and to the CO₂ phase from 296°C to 329°C (type IIa, 287°C; type IIb, 303

to 309°C, Fig. 7b). Their bulk densities range from 0.35 to 0.85 g/cm³.

Type III inclusions also form CO₂ solid upon cooling. Their *T_m* was 56.6°C, inferring a phase of solely CO₂. Th-CO₂ values vary from 30.6°C to 30.7°C (Table 1).

Stable isotopes

Thirty-seven sulfide mineral separates were analyzed for sulfur isotope composition (Table 2). δ³⁴S values of sulfide minerals from the Xihuashan deposit vary in a relatively narrow range of -1.6 to +0.1‰ (Fig. 8). δ¹⁸O values of wolframite range from +4.8‰ to +6.3‰ with an average of +5.5‰ (Table 3).

Fig. 7 Histograms of CO₂ homogenization temperatures (Th_{CO2}) and total homogenization temperatures (Th_{total}) of type II inclusions in quartz at Xihuashan

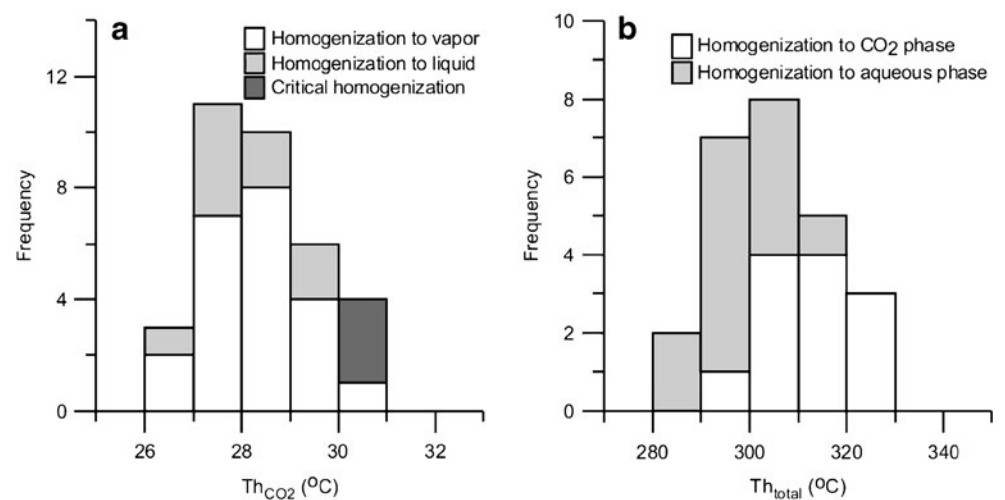


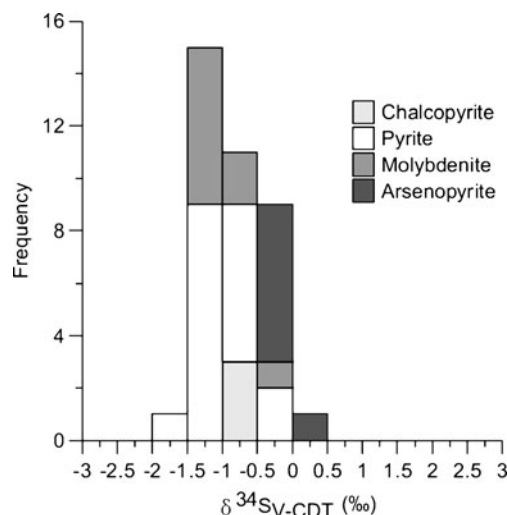
Table 2 $\delta^{34}\text{S}$ values of various sulfide minerals of the Xihuashan tungsten deposit

Sample	Minerals	$\delta^{34}\text{S}_{\text{CDT}}$ (‰)
378-6	Pyrite	-1.0
378-9	Pyrite	-1.0
378-11	Pyrite	-1.6
378-5	Pyrite	-1.2
270-5	Pyrite	-0.9
270-4	Pyrite	-1.1
270-10	Pyrite	-1.2
270-13	Pyrite	-1.3
270-23	Pyrite	-1.3
431-3	Pyrite	-1.4
431-4	Pyrite	-1.2
538-4	Pyrite	-1.0
538-10	Pyrite	-1.3
538-20	Pyrite	-0.7
538-9	Pyrite	-0.8
431-5	Pyrite	-1.4
270-28	Molybdenite	-0.9
378-20	Molybdenite	-1.4
378-19	Molybdenite	-1.4
378-17	Molybdenite	-1.2
378-34	Molybdenite	-1.4
378-35	Molybdenite	-0.8
431-1	Molybdenite	-1.4
431-6	Molybdenite	-1.1
431-7	Molybdenite	-0.5
538-3	Arsenopyrite	+0.1
538-9	Arsenopyrite	-0.2
538-11	Arsenopyrite	-0.1
538-12	Arsenopyrite	-0.1
538-18	Arsenopyrite	0.0
270-9	Arsenopyrite	-0.2
431-32	Arsenopyrite	-0.2
538-14	Chalcopyrite	-0.7
538-9	Chalcopyrite	-0.7
538-7	Chalcopyrite	-0.4
538-5	Chalcopyrite	-0.3
538-4	Chalcopyrite	-0.6

Discussion

Comparison of fluid inclusions in wolframite and quartz

Fluid inclusions in wolframite and quartz from Xihuashan have remarkably different temperatures and salinities. There are also differences between minerals in the same sample (e.g., 431–22, 431–23, 483–4). Homogenization temperatures of fluid inclusions of wolframite are mostly higher

**Fig. 8** Histogram displaying the sulfur isotope composition of various sulfides from the Xihuashan deposit, southern Jiangxi

than those of fluid inclusions in quartz from the silicate-oxide stage. The mineralizing fluids entrapped in wolframite are moderate to high-salinity solutions.

At Xihuashan, halite-bearing inclusions and coexisting aqueous inclusions homogenize both to vapor and liquid at similar temperatures, indicating boiling (Sheng 1985; Wu et al. 1987). Two- or three-phase CO_2 -rich inclusions and two-phase pure CO_2 inclusions always coexist with two-phase aqueous inclusions in quartz, with similar homogenization temperatures, indicative of fluid boiling (e.g., Fig. 5i–k; Roedder 1984; So and Yun 1994; Lu et al. 2004) in the silicate-oxide stage. Thus, at least one episode of boiling probably occurred during hydrothermal mineralization leading to the formation of type II and III inclusions trapped in quartz.

On the other hand, two- or three-phase CO_2 -rich inclusions or vapor-rich inclusions are not present in wolframite from Xihuashan. Furthermore, wolframite occurs in the vein walls and quartz in the vein centers, which is the textural evidence for wolframite relatively

Table 3 $\delta^{18}\text{O}$ values of Wolframite in the Xihuashan tungsten deposit

Sample	Minerals	$\delta^{18}\text{O}_{\text{V-SMOW}}\%$
230-12	Wolframite	+5.8
270-2	Wolframite	+5.7
270-31	Wolframite	+6.3
378-43	Wolframite	+5.2
378-45	Wolframite	+4.9
431-22	Wolframite	+4.8
431-24	Wolframite	+5.4
483-4	Wolframite	+5.9
483-6	Wolframite	+5.7

preceding quartz paragenetically (Fig. 4b). The data obtained from fluid inclusions also indicate that wolframite was deposited prior to quartz under higher temperatures from high-salinity fluids. Therefore, although there was an episode of boiling during the vein mineralization process, boiling of the ore-forming fluids seems to occur after wolframite deposition and did not play an important role for wolframite precipitation. Although CO₂-rich inclusions are not observed in wolframite, the possibility that aqueous fluid inclusions contain trace amounts of dissolved CO₂ or CH₄ (Roedder 1984; Hagemann and Lüders 2003) cannot be excluded. Furthermore, fluid inclusion volatile analysis by gas chromatography implies that fluid inclusions in wolframite contain trace amounts of CO₂ (Wu et al. 1987).

Fluid evolution

During the silicate-oxide stage, the relatively low salinities in fluid inclusions of both wolframite and quartz suggest lower salinity fluids. Boiling cannot yield such a fluid. Instead, it can cause a gradual and slight increase in salinity of the liquid phase (So and Yun 1994). The lower salinities may be ascribed to mixing. The homogenization temperature–salinity plot (Fig. 9) clearly shows a trend of dilution, evidence for mixing between a hot, saline fluid and a cooler, dilute fluid (Chi and Savard 1997). Evidence of mixing also includes the appearance of groups of relatively low-salinity aqueous inclusions close to isolated high-salinity aqueous inclusions (Zoheir et al. 2008).

Fluid inclusions suggesting fluid boiling are common in tungsten deposits (Giamello et al. 1992; Smith et al. 1996). Our results and previous studies (Sheng 1985; Giuliani et al. 1988) provide evidence for the occurrence of boiling in

Xihuashan. In this observation, it is difficult to define exactly the initial hydrothermal fluid before boiling. However, according to Giuliani et al. (1988), the earlier low-density and low-salinity CO₂-bearing aqueous solutions may represent the initial hydrothermal fluid before boiling. During boiling, the dissolved gas (e.g., CO₂, CH₄) would be separated from the fluids, producing two- or three-phase CO₂-rich inclusions, leaving a residual liquid of only very low CO₂ content which may be represented by some type I inclusions in quartz. The process of CO₂ separation together with spatial separation of the fluids could give birth to a ‘refining’ effect that causes the entrapment of pure CO₂ inclusions (Johnson and Hollister 1995). As a result of fluid boiling, drastic fluctuating CO₂ contents can be observed in which two-phase pure CO₂ inclusions grade into three-phase CO₂-rich inclusions (Fig. 5j).

During the sulfide stage, salinities of aqueous inclusions in quartz are relatively low. Decreasing salinities are likely attributed to mixing. Furthermore, mixing of fluids is implied from the relationship between homogenization temperatures and salinities of aqueous inclusions (Fig. 9).

Estimation of pressure during boiling

Fluid inclusions trapped during boiling can be used for accurate estimating fluid temperature and pressure (Ruggieri et al. 1999; Yoo et al. 2010). Homogenization temperatures of coexisting boiling type I, II, and III inclusions are equal to the fluid trapping temperature. Isochores for the type I aqueous inclusions in quartz from the silicate-oxide stage were calculated with the equation of state for H₂O–NaCl of Zhang and Frantz (1987). Isochores of type II and III inclusions were estimated using the equation of state for NaCl–H₂O–CO₂ or CO₂ of Bowers and Helgeson (1983) and Brown (1989). Based on fluid inclusion compositions, calculated isochores of type I and II inclusions are shown in Fig. 10. At 329°C, the highest homogenization temperature for type II inclusions coexisting with type I inclusions from the silicate-oxide stage, isochores of type II inclusions indicate a pressure range from 600 to 750 bars. The pressure range is from 252 to 683 bars on the basis of isochore calculations at a temperature of 300°C, the average homogenization temperature of fluid inclusions for samples 538-5 and 538-14 from the silicate-oxide stage. This range is consistent with the pressure of 300–700 bars obtained by Lu (1986).

Enthalpy–salinity relationship

Plots of enthalpy and salinity are useful for evaluating fluid mixing and boiling processes of ascendant hydrothermal fluids (Hedenquist 1990; Hayba 1997; Wilkinson 2001). An enthalpy–salinity plot for the Xihuashan deposit is shown

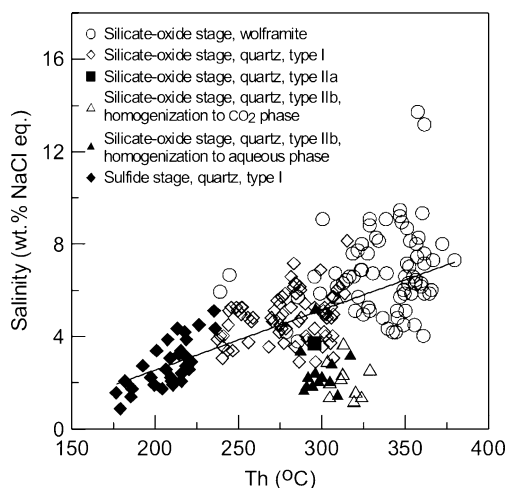


Fig. 9 Homogenization temperature versus salinity of different types of fluid inclusions in wolframite and quartz at Xihuashan deposit

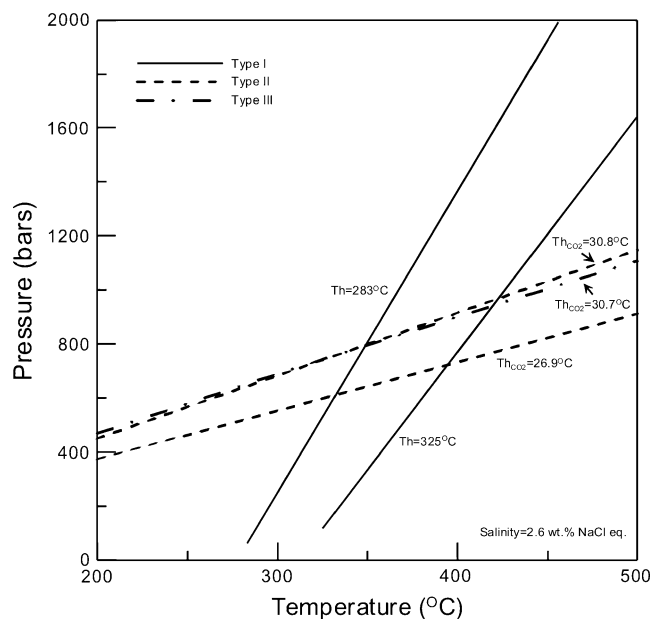


Fig. 10 P - T diagram isochores for type I, II, and III inclusions under boiling conditions in the Xihuashan tungsten deposit. 283°C, the average homogenization temperature of type I inclusions in quartz from silicate-oxide stage. 2.6 wt.% NaCl eq., the average salinity of type II inclusions in quartz from silicate-oxide stage

in Fig. 11. The enthalpy values of the fluids within the studied inclusions were calculated according to the online calculation program (<http://geotherm.ucsd.edu>). Although boiling occurred during the silicate-oxide stage in Xihuashan, it is impossible to explain the changes of enthalpy and salinity by boiling. Mixing may decrease both salinity and enthalpy, whereas boiling decreases only enthalpy but increases salinity (Wilkinson 2001). Therefore, fluid mixing can be estimated from a positive correlation between enthalpy and salinity shown in Fig. 11. The mixing may have provided a mechanism for the deposition of wolframite.

Sources of ore-forming fluids

Sulfides from the Xihuashan deposit have quite homogeneous $\delta^{34}\text{S}$ values (Fig. 8), in agreement with previously published data ($\delta^{34}\text{S}=-2.3$ to $+2.4\%$; Zhang et al. 1981). These rather uniform values indicate igneous sulfur and point to a large-scale hydrothermal system with a homogeneous source of sulfur, which was likely of magmatic origin and magmatic sulfur directly mingling into a fluid system (Wagner et al. 2005, 2009). According to Mu et al. (1981), Zhang et al. (1981), and Liu et al. (2002), quartz at Xihuashan has δD values of -43% to -81% for water extracted from fluid inclusions and the $\delta^{18}\text{O}$ values of -8.8% to $+8.4\%$ for water in equilibrium with quartz. This composition could be reasonably explained by the mixing of magmatic water with meteoric water.

The role of boiling and mixing for tungsten mineralization

In order to further constrain the origin of the mineralization, we have quantitatively modeled the isotopic effects of boiling and mixing (Fig. 12) using $\delta^{18}\text{O}$ values of minerals by the method of Wagner et al. (2009). The calculations have employed the mineral-water isotope fractionation equation of Matsuhisa et al. (1979) and Zhang et al. (1994). The equilibrium temperature was assumed to be 380°C which is the highest homogenization temperature of fluid inclusions in wolframite. For the calculations, we have chosen the $\delta^{18}\text{O}$ values of -8.1% for meteoric water, which represents the oxygen isotope composition of Mesozoic meteoric waters at Xihuashan and of $+10.1\%$ for the magmatic end member, which represents the $\delta^{18}\text{O}$ value for water in equilibrium with quartz of the biotite granite at Xihuashan (Chen and Zhang 1990). Mixing models have been calculated for the temperatures of the meteoric water for 200°C, 150°C, 100°C, 50°C, respectively. In Fig. 12a, a rectangle represents the measured values of wolframite and the main range of fluid inclusion homogenization temperatures in wolframite. In Fig. 12b, a rectangle represents the $\delta^{18}\text{O}$ data ($+10.4\%$ to $+13\%$) of quartz in the silicate-oxide stage reported by Zhang et al. (1981) and our fluid inclusion homogenization temperatures in quartz. It is obvious that, instead of boiling, mixing can explain the observed relationship between fluid inclusion temperatures and $\delta^{18}\text{O}$ values of wolframite. The mass fractions of meteoric water during the silicate-oxide stage were about 0.1–0.4. Although there is evidence for boiling from fluid inclusions in quartz, local boiling (Giuliani et al. 1988) is probably less important for the evolution of the hydrothermal system at Xihuashan. As a dominant ore-forming process, mixing between magmatic and meteoric fluids may have resulted in the deposition of wolframite.

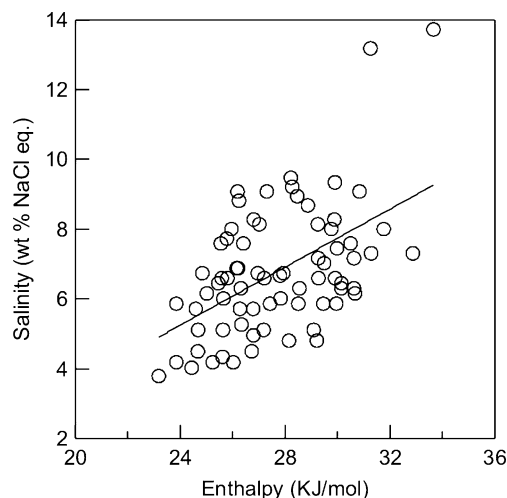
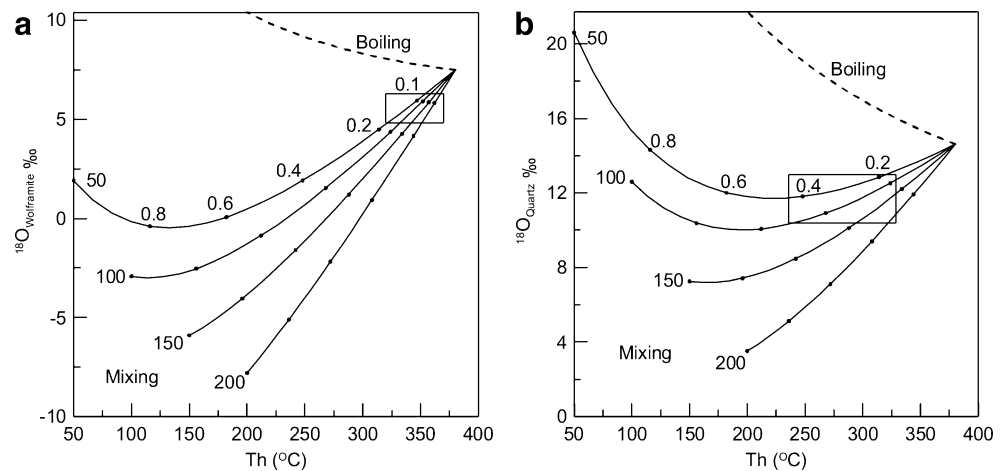


Fig. 11 Enthalpy–salinity plot for fluid inclusions in wolframite from Xihuashan

Fig. 12 Diagram showing the effect of boiling and mixing on the oxygen isotope composition of wolframite and quartz precipitated from hydrothermal fluids at different temperatures. Numbers are mass fraction of meteoric water



Fluid mixing and mineral deposition

Experimental studies and thermodynamic modeling show that salty, reduced, and acidic solutions have the highest solubility for tungsten and that tungsten is transported in ore fluids as simple tungstate species (i.e., H_2WO_4 , HWO_4^- , WO_4^{2-}), and alkali-tungstate ion pairs (Wood and Samson 2000; Gong et al. 2004). Therefore, the precipitation of tungsten results from increase of pH and oxygen fugacity as well as decrease of temperature and chloride concentration. Possible mechanisms for wolframite deposition may include pressure decrease, wall-rock alteration, boiling, and fluid mixing (Ramboz et al. 1985; Polya 1989; So and Yun 1994; O'Reilly et al. 1997; Yokart et al. 2003; Beuchat et al. 2004; Gong et al. 2004). In Xihuashan, wolframite occurs mainly within quartz veins, where wall-rock alteration is limited (Zhao et al. 1998). Thus, wall-rock alteration can be excluded as an effective mechanism for wolframite deposition. Structural evidence for a transition from a closed to open vein system suggests a pressure decrease during crystallization (Wu et al. 1987). Pressure fluctuations have a dramatic effect on the wolframite solubility (Polya 1990). However, recent study suggests that wolframite solubility is only weakly dependent on pressure (Wood and Samson 2000). Consequently, a pressure decrease would not have been an effective cause of wolframite deposition in Xihuashan.

A number of numerical modelings (Drummond and Ohmoto 1985) and laboratory studies (Sondergeld and Turcotte 1979) emphasize the importance of boiling phenomena during ore deposition. Boiling has been considered as the most efficient mechanism for wolframite precipitation at several tungsten deposits (Higgins 1985; So and Yun 1994). In Xihuashan, fluid inclusions in quartz from the silicate-oxide stage show evidence of fluid boiling during mineralization. Boiling would decrease temperature but increase pH of the fluid. Accordingly, it could promote the precipitation of wolframite. However, in some deposits,

the effect of boiling has been overemphasized (Roedder 1984; Hayba 1997). No unambiguous evidence for boiling was observed in the wolframite-hosted fluid inclusions from Xihuashan. In addition, the boiling temperatures for quartz are lower. Consequently, the absence of two- or three-phase CO_2 -rich or vapor-rich inclusions in wolframite may be attributed to wolframite precipitation prior to the boiling of the ore-forming fluids. Boiled fluid inclusions in quartz are rare but may be present locally (Giuliani et al. 1988). Even if boiling occurred, the extent was probably limited. Moreover, because vapor separation leads to a relative depletion in D of residual fluids, boiling could have influenced the hydrogen isotope composition of the fluids (Kodera et al. 2005; Yoo et al. 2010). However, this is not apparent in the measured δD values in Xihuashan (Liu et al. 2002). Therefore, limited fluid boiling does not appear to be an effective tungsten mineralizing process in Xihuashan. During the silicate-oxide stage, temperatures (from 236°C to 380°C) and salinities (from 1.2 to 13.7 wt.% NaCl equiv) show considerable fluctuations, suggesting fluid mixing. Boiling inclusions have low pressures, corresponding to shallow depths and consequently the involvement of meteoric water (Neiva 2008). Furthermore, most of the measured isotope compositions indicated the mixing of two fluids, meteoric water, and magmatic hydrothermal fluids (Mu et al. 1981; Liu et al. 2002).

Quantification of boiling and fluid mixing mechanisms of ore formation also shows that boiling is not a major process in the evolution of the ore-forming fluid. Instead, mixing of magmatic and meteoric waters coincides with the observed $\delta^{18}\text{O}$ values of wolframite and quartz. Therefore, mixing of meteoric water and tungsten-bearing magmatic fluids led to oxidation, decrease in temperature and chloride concentration, increased pH, and finally led to the precipitation of wolframite. Numerical thermodynamic modeling also indicates that boiling does not affect wolframite precipitation, whereas mixing of meteoric waters and deep-seated ore-bearing solutions leads to wolframite

precipitation (Bychkov and Matveeva 2008; Sushchevskaya and Bychkov 2009). Thus, fluid mixing, rather than boiling, can best explain the formation of wolframite at Xihuashan.

Conclusions

1. Wolframite and quartz from the Xihuashan tungsten deposit did not co-precipitate. Wolframite deposition seems to occur prior to quartz deposition and boiling of the ore-forming fluid. Boiling of the ore fluids occurred during quartz precipitation.
2. Mixing between a dominantly magmatic fluid and a minor meteoric fluid is the main metallogenic mechanism associated with wolframite precipitation in the Xihuashan tungsten deposit.
3. Quantitative modeling of isotopic compositions of wolframite and quartz show that mass fractions of the meteoric water in the mixed fluid were between 0.1 and 0.4 during the silicate-oxide stage.
4. Differences in fluid inclusions from wolframite and quartz demonstrate that the conventional microthermometric data from gangue minerals cannot be used for simple extrapolating the depositional conditions of associated ore minerals.

Acknowledgements The authors give special thanks to geologists for helpful field assistance. Discussions with and advice from Mei-Fu Zhou, Huanzhang Lu, Chen Zhu, and Hong Zhong are appreciated. Our thanks are also due to Volker Lüders, an anonymous reviewer, and Bernd Lehmann for their careful and constructive comments and suggestions, which significantly improved the manuscript. This work was financially supported by the National Basic Research Program of China (Grant No 2007CB411400, 2007CB411404, 2007CB411408) and the Chinese Academy of Sciences Innovative Program (Grant No KZCX2-YW-Q04).

References

- Bailly L, Grancea L, Kouzmanov K (2002) Infrared microthermometry and chemistry of wolframite from the Baia Sprie epithermal deposit, Romania. *Econ Geol* 97:415–423
- Beuchat S, Moritz R, Pettke T (2004) Fluid evolution in the W-Cu-Zn-Pb San Cristobal vein, Peru: fluid inclusion and stable isotope evidence. *Chem Geol* 210:201–224
- Bowers TS, Helgeson HC (1983) Calculation of the thermodynamic and geochemical consequences of nonideal mixing in the system H_2O-CO_2-NaCl on phase relations in geologic systems: equation of state for H_2O-CO_2-NaCl fluids at high pressures and temperatures. *Geochim Cosmochim Acta* 47:1247–1275
- Brown PE (1989) FLINCOR: a microcomputer program for the reduction and investigation of fluid-inclusion data. *Am Miner* 74:1390–1393
- Burnard PG, Polya DA (2004) Importance of mantle derived fluids during granite associated hydrothermal circulation: He and Ar isotopes of ore minerals from Panasqueira. *Geochim Cosmochim Acta* 68:1607–1615
- Bychkov A, Matveeva S (2008) Thermodynamic model of the formation of ore bodies at the Akchatau wolframite greisen-vein deposit. *Geochem Int* 46:867–886
- Campbell AR, Panter KS (1990) Comparison of fluid inclusions in coexisting (cogenetic?) wolframite, cassiterite, and quartz from St. Michael's Mount and Cligga Head, Cornwall, England. *Geochim Cosmochim Acta* 54:673–681
- Campbell AR, Hackbarth CJ, Plumlee GS, Petersen U (1984) Internal features of ore minerals seen with the infrared microscope. *Econ Geol* 79:1387–1392
- Cao XF, Lü XB, He MC, Niu H, Du BF, Mei W (2009) An infrared microscope investigation of fluid inclusions in coexisting quartz and wolframite: a case study of Yaogangxian quartz-vein wolframite deposit (in Chinese with English abstract). *Miner Depos* 28:611–620
- Chang HL, Wang XW, Wang XD, Liu JQ, Huang HL (2007) The composition of melt inclusions in beryl from wolframite-quartz veins in Xihuashan, Jiangxi Province (in Chinese with English abstract). *Acta Petrol ET Mineral* 26:259–268
- Chen JF, Jahn BM (1998) Crustal evolution of southeastern China: Nd and Sr isotopic evidence. *Tectonophysics* 284:101–133
- Chen ZS, Zhang LG (1990) Hydrogen and oxygen isotope study on altered rocks and its geological significance: with the example of Xihuashan tungsten ore deposit (in Chinese with English abstract). *Contrib Geol Miner Resour Res* 5:69–79
- Chi GX, Savard M (1997) Sources of basinal and Mississippi Valley-type mineralizing brines: mixing of evaporated seawater and halite-dissolution brine. *Chem Geol* 143:121–125
- Clayton RN, Mayeda TK (1963) The use of bromine pentafluoride in the extraction of oxygen from oxides and silicates for isotopic analysis. *Geochim Cosmochim Acta* 27:43–52
- Drummond SE, Ohmoto H (1985) Chemical evolution and mineral deposition in boiling hydrothermal systems. *Econ Geol* 80:126–147
- Duan ZH, Moller N, Weare JH (1995) Equation of state for the $NaCl-H_2O-CO_2$ system: prediction of phase equilibria and volumetric properties. *Geochim Cosmochim Acta* 59:2869–2882
- Fan CF, Chen PR (2000) Geochemical characteristics and tectonic implication of Beitou A-type granitic intrusives in South Jiangxi Province (in Chinese with English abstract). *Geochimica* 29:358–366
- Giamello M, Protano G, Riccobono F, Sabatini G (1992) The W-Mo deposit of Perda Majori (SE Sardinia, Italy): a fluid inclusion study of ore and gangue minerals. *Eur J Miner* 4:1079–1084
- Giuliani G (1985) Le gisement de tungstène de Xihuashan (Sud-Jiangxi, Chine): relations granites, altérations deutériques-hydrothermales, minéralisations. *Miner Depos* 20:107–115
- Giuliani G, Li YD, Sheng TF (1988) Fluid inclusion study of Xihuashan tungsten deposit in the southern Jiangxi Province, China. *Miner Depos* 23:24–33
- Goldstein RH, Reynolds TJ (1994) Systematics of fluid inclusions in diagenetic minerals. *SEPM Short C* 31:1–199
- Gong QJ, Yu CW, Zhang RH (2004) Physical chemistry study on the ore-forming process of Shizhuoyuan tungsten-polymetallic deposit (in Chinese with English abstract). *Earth Sci Front* 11:617–625
- Grassineau NV, Matthey DP, Lowry D (2001) Sulfur isotope analysis of sulfide and sulfate minerals by continuous flow-isotope ratio mass spectrometry. *Anal Chem* 73:220–225
- Graupner T, Kempe U, Dombon E, Pätzold O, Leeder O, Spooner ETC (1999) Fluid regime and ore formation in the tungsten (–yttrium) deposits of Kyzyltau (Mongolian Altai): evidence for fluid variability in tungsten-tin ore systems. *Chem Geol* 154:21–58
- Gu XX, Schulz O, Vavtar F, Liu JM, Zheng MH, Fu SH (2007) Rare earth element geochemistry of the Woxi W-Sb-Au deposit, Hunan Province, South China. *Ore Geol Rev* 31:319–336

- Hagemann S, Lüders V (2003) P-T-X conditions of hydrothermal fluids and precipitation mechanism of stibnite-gold mineralization at the Wiluna lode-gold deposits, Western Australia: conventional and infrared microthermometric constraints. *Miner Depos* 38:936–952
- Hayba DO (1997) Environment of ore deposition in the Creede mining district, San Juan Mountains, Colorado: Part V. Epithermal mineralization from fluid mixing in the OH Vein. *Econ Geol* 92:29–44
- Hedenquist JW (1990) The thermal and geochemical structure of the Broadlands-Ohaaki geothermal system, New Zealand. *Geothermics* 19:151–185
- Heinrich CA (1990) The chemistry of hydrothermal tin(–tungsten) ore deposition. *Econ Geol* 85:457–481
- Higgins NC (1985) Wolframite deposition in a hydrothermal vein system: the Grey River tungsten prospect, Newfoundland, Canada. *Econ Geol* 80:1297–1327
- Hsieh PS, Chen CH, Yang HJ, Lee CY (2008) Petrogenesis of the Nanling Mountains granites from South China: constraints from systematic apatite geochemistry and whole-rock geochemical and Sr–Nd isotope compositions. *J Asian Earth Sci* 33:428–451
- Hu RZ, Bi XW, Zhou MF, Peng JT, Su WC, Liu S, Qi HW (2008) Uranium metallogenesis in South China and its relationship to crustal extension during the Cretaceous to Tertiary. *Econ Geol* 103:583–598
- Johnson EL, Hollister LS (1995) Syndeformational fluid trapping in quartz: determining the pressure-temperature conditions of deformation from fluid inclusions and the formation of pure CO₂ fluid inclusions during grain-boundary migration. *J Metamorph Geol* 13:239–249
- Kelly WC, Rye RO (1979) Geologic, fluid inclusion, and stable isotope studies of the tin-tungsten deposits of Panasqueira, Portugal. *Econ Geol* 74:1721–1822
- Koděra P, Lexa J, Rankin AH, Fallick AE (2005) Epithermal gold veins in a caldera setting: Banská Hôrduša, Slovakia. *Miner Depos* 39:921–943
- Kouzmanov K, Ramboz C, Bailly L, Bogdanov K (2004) Genesis of high-sulfidation vinciennite-bearing Cu–As–Sn (<Au) assemblage from the Radka epithermal copper deposit, Bulgaria: evidence from mineralogy and infrared microthermometry of enargite. *Can Miner* 42:1501–1521
- Kucha H, Raith JG (2009) Gold-oxysulphides in copper deposits of the Greywacke Zone, Austria: a mineral chemical and infrared fluid inclusion study. *Ore Geol Rev* 35:87–100
- Landis GP, Rye RO (1974) Geologic, fluid inclusion, and stable isotope studies of the Pasto Buena tungsten-base metal ore deposit, Northern Peru. *Econ Geol* 69:1025–1059
- Le Bel L, Li YD, Sheng JF (1984) Granitic evolution of the Xihuashan-Dangping (Jiangxi, China) tungsten-bearing system. *Miner Pet* 33:149–167
- Li XH, Li WX, Wang XC, Li QL, Liu Y, Tang GQ (2009) Role of mantle-derived magma in genesis of early Yanshanian granites in the Nanling Range, South China: in situ zircon Hf–O isotopic constraints. *Sci China Ser D Earth Sci* 52:1262–1278
- Lindaas SE, Kulis J, Campbell AR (2002) Near-infrared observation and microthermometry of pyrite-hosted fluid inclusions. *Econ Geol* 97:603–618
- Liu JQ, Wang XW, Zeng YS, Wang XD (2002) Xihuashan granite and evolution of ore-forming fluid of tungsten-tin-beryllium ore field (in Chinese with English abstract). *Geology and Mineral Resources of South China*: 91–96
- Lu HZ (1986) The origin of tungsten mineral deposits in south China (in Chinese). Chongqing Publishing House, Chongqing, pp 1–232
- Lu HZ, Liu YM, Wang CL, Xu YZ, Li HQ (2003) Mineralization and fluid inclusion study of the Shizhuyuan W–Sn–Bi–Mo–F skarn deposit, Hunan Province, China. *Econ Geol* 98:955–974
- Lu HZ, Fan HR, Ni P, Ou GX, Shen K, Zhang WH (2004) Fluid inclusion (in Chinese). Science Press, Beijing, pp 1–487
- Lüders V (1996) Contribution of infrared microscopy to fluid inclusion studies in some opaque minerals (wolframite, stibnite, bournonite): metallogenic implications. *Econ Geol* 91:1462–1468
- Lüders V, Ziemann M (1999) Possibilities and limits of infrared light microthermometry applied to studies of pyrite-hosted fluid inclusions. *Chem Geol* 154:169–178
- Lüders V, Gutzmer J, Beukes NJ (1999) Fluid inclusion studies in cogenetic hematite, hausmannite, and gangue minerals from high-grade manganese ores in the Kalahari manganese field, South Africa. *Econ Geol* 94:589–595
- Lüders V, Romer R, Cabral A, Schmidt C, Banks D, Schneider J (2005) Genesis of itabirite-hosted Au–Pd–Pt-bearing hematite-(quartz) veins, Quadrilátero Ferrífero, Minas Gerais, Brazil: constraints from fluid inclusion infrared microthermometry, bulk crush-leach analysis and U–Pb systematics. *Miner Depos* 40:289–306
- Lüders V, Romer RL, Gilg HA, Bodnar RJ, Pettke T, Misantoni D (2009) A geochemical study of the Sweet Home Mine, Colorado Mineral Belt, USA: hydrothermal fluid evolution above a hypothesized granite cupola. *Miner Depos* 44:415–434
- Macey P, Harris C (2006) Stable isotope and fluid inclusion evidence for the origin of the Brandberg West area Sn–W vein deposits, NW Namibia. *Miner Depos* 41:671–690
- Mancano DP, Campbell AR (1995) Microthermometry of enargite-hosted fluid inclusions from the Lepanto, Philippines, high-sulfidation Cu–Au deposit. *Geochim Cosmochim Acta* 59:3909–3916
- Mao JW, Xie GQ, Guo CL, Chen YC (2007) Large-scale tungsten-tin mineralization in the Nanling region, South China: metallogenic ages and corresponding geodynamic processes (in Chinese with English abstract). *Acta Petrol Sinica* 23:2329–2338
- Marujól P, Cuney M, Turpin L (1990) Magmatic and hydrothermal R. E.E. fractionation in the Xihuashan granites (SE China). *Contrib Miner Petrol* 104:668–680
- Matsuhisa Y, Goldsmith JR, Clayton RN (1979) Oxygen isotopic fractionation in the system quartz–albite–anorthite–water. *Geochim Cosmochim Acta* 43:1131–1140
- McKee EH, Rytuba JJ, Xu K, Giuliani G (1987) Geochronology of the Xihuashan composite granitic body and tungsten mineralization, Jiangxi Province, South China. *Econ Geol* 82:218–223
- Mo SZ, Ye BD, Pang WZ, Wan SN (1980) Granitoid geology in the Nanling region (in Chinese). Geological Publishing House, Beijing, pp 115–180
- Moritz R (2006) Fluid salinities obtained by infrared microthermometry of opaque minerals: implications for ore deposit modeling—a note of caution. *J Geochem Explor* 89:284–287
- Mu ZG, Huang FS, Chen CY, Zheng SH, Fan SL, Liu DR, Mei YW (1981) Oxygen, hydrogen and carbon isotope studies of Piaotang and Xihuashan quartz vein-type tungsten deposits, Jiangxi Province (in Chinese). *Proceedings of Symposium on Tungsten Geology*. Geological Publishing House, Beijing, pp 153–169
- Neiva AMR (2008) Geochemistry of cassiterite and wolframite from tin and tungsten quartz veins in Portugal. *Ore Geol Rev* 33:221–238
- Ni P, Zhu X, Wang RC, Shen K, Zhang ZM, Qiu JS, Huang JP (2008) Constraining ultrahigh-pressure (UHP) metamorphism and titanium ore formation from an infrared microthermometric study of fluid inclusions in rutile from Donghai UHP eclogites, eastern China. *GSA Bull* 120:1296–1304
- O’Reilly C, Gallagher V, Feely M (1997) Fluid inclusion study of the Ballinglen W–Sn-sulphide mineralization, SE Ireland. *Miner Depos* 32:569–580
- Peng JT, Zhou MF, Hu RZ, Shen NP, Yuan SD, Bi XW, Du AD, Qu WJ (2006) Precise molybdenite Re–Os and mica Ar–Ar dating of the

- Mesozoic Yaogangxian tungsten deposit, central Nanling district, South China. *Miner Depos* 41:661–669
- Petrunic BM, Al TA (2005) Mineral/water interactions in tailings from a tungsten mine, Mount Pleasant, New Brunswick. *Geochim Cosmochim Acta* 69:2469–2483
- Polya DA (1989) Chemistry of the main-stage ore-forming fluids of the Panasqueira W-Cu(Ag)-Sn deposit, Portugal: implications for models of ore genesis. *Econ Geol* 84:1134–1152
- Polya DA (1990) Pressure-dependence of wolframite solubility for hydrothermal vein formation. *Trans Inst Min Metall Sect B-Appl Earth Sci* 99:B120–B124
- Polya DA, Foxford KA, Stuart FM, Boyce A, Fallick AE (2000) Evolution and paragenetic context of low δD hydrothermal fluids from the Panasqueira W-Sn deposit, Portugal: new evidence from microthermometric, stable isotope, noble gas and halogen analyses of primary fluid inclusions. *Geochim Cosmochim Acta* 64:3357–3371
- Ramboz C, Schnapper D, Dubessy J (1985) The evolution of H₂O-CO₂-CH₄-bearing fluid in a wolframite vein: reconstruction from fluid inclusion studies. *Geochim Cosmochim Acta* 49:205–219
- Rice CM, Harmon RS, Boyce AJ, Fallick AE (2001) Assessment of grid-based whole-rock δD surveys in exploration: Boulder County epithermal tungsten deposit, Colorado. *Econ Geol* 96:133–143
- Richards J, Kerrich R (1993) Observations of zoning and fluid inclusions in pyrite using a transmitted infrared light microscope ($\lambda \leq 1.9 \mu m$). *Econ Geol* 88:716–723
- Rios FJ, Villas RN, Fuzikawa K (2003) Fluid evolution in the Pedra Preta wolframite ore deposit, Paleoproterozoic Musa granite, eastern Amazon craton, Brazil. *J S Am Earth Sci* 15:787–802
- Rios FJ, Alves JV, Perez CA, Costa EC, Rosiere CA, Fuzikawa K, Correia Neves JM, DeOchaves A, Prates SP, De Barrio RE (2006) Combined investigations of fluid inclusions in opaque ore minerals by NIR/SWIR microscopy and microthermometry and synchrotron radiation X-ray fluorescence. *Appl Geochem* 21:813–819
- Roedder E (1984) Fluid inclusions. *Miner Soc Am Rev Miner* 12:1–644
- Rosiere CA, Rios FJ (2004) The origin of hematite in high-grade iron ores based on infrared microscopy and fluid inclusion studies: the example of the Conceicao mine, Quadrilatero Ferrifero, Brazil. *Econ Geol* 99:611–624
- Ruggieri G, Cathelineau M, Boiron M-C, Marignac C (1999) Boiling and fluid mixing in the chlorite zone of the Larderello geothermal system. *Chem Geol* 154:237–256
- Rusk BG, Reed MH, Dilles JH (2008) Fluid inclusion evidence for magmatic-hydrothermal fluid evolution in the porphyry copper-molybdenum deposit at Butte, Montana. *Econ Geol* 103:307–334
- Samson IM (1990) Fluid evolution and mineralization in a sub-volcanic granite stock: the Mount Pleasant W-Mo-Sn deposits, New Brunswick, Canada. *Econ Geol* 85:145–163
- Shen WZ, Xu SJ, Wang YX, Yang JD (1994) Study on the Nd-Sr isotope of the Xihuashan granite (in Chinese with English abstract). *Chin Sci Bull* 39:154–156
- Sheng JF (1985) A study of fluid inclusions and metallogenesis of the Xihuashan tungsten deposit (in Chinese with English abstract). *Bull Inst Miner Depos Chin Acad Geol Sci* 2:44–61
- Smith M, Banks DA, Yardley BWD, Boyce AJ (1996) Fluid inclusion and stable isotope constraints on the genesis of the Cligga Head Sn-W deposit, S.W. England. *Eur J Miner* 8:961–974
- So CS, Yun ST (1994) Origin and evolution of W-Mo-producing fluids in a granitic hydrothermal system: geochemical studies of quartz vein deposits around the Susan Granite, Hwanggangri District, Republic of Korea. *Econ Geol* 89:246–267
- Sondergeld CH, Turcotte DL (1979) A laboratory study of mineral deposition in a boiling environment. *Econ Geol* 74:109–115
- Sushchevskaya TM, Bychkov AJ (2009) Thermodynamic modeling of cassiterite-wolframite ore formation at the Iultin Sn-W deposit. *Geochim Cosmochim Acta* 73:A1296–A1296
- Tanelli G (1982) Geological setting, mineralogy and genesis of tungsten mineralization in Dayu district, Jiangxi (People's Republic of China): an outline. *Miner Depos* 17:279–294
- USGS (2010) U.S. Geological survey mineral commodity summaries. Tungsten: 176–177
- Wagner T, Williams-Jones AE, Boyce AJ (2005) Stable isotope-based modeling of the origin and genesis of an unusual Au-Ag-Sn-W epithermal system at Cirotan, Indonesia. *Chem Geol* 219:237–260
- Wagner T, Mlynarczyk MSJ, Williams-Jones AE, Boyce AJ (2009) Stable isotope constraints on ore formation at the San Rafael tin-copper deposit, Southeast Peru. *Econ Geol* 104:223–248
- Wang RC, Fontan F, Chen XM, Hu H, Liu CS, Xu SJ, De Parseval P (2003) Accessory minerals in the Xihuashan Y-enriched granitic complex, Southern China: a record of magmatic and hydrothermal stages of evolution. *Can Miner* 41:727–748
- Wilkinson JJ (2001) Fluid inclusions in hydrothermal ore deposits. *Lithos* 55:229–272
- Wood SA, Samson IM (2000) The hydrothermal geochemistry of tungsten in granitoid environments: I. Relative solubilities of ferberite and scheelite as a function of T, P, pH, and m_{NaCl} . *Econ Geol* 95:143–182
- Wu YL, Mei YW, Liu PC, Cai CL, Lu TY (1987) Geology of the Xihuashan tungsten ore field (in Chinese). Geological Publishing House, Beijing, pp 1–317
- Wu FY, Li XH, Yang JH, Zheng YF (2007) Discussions on the petrogenesis of granites (in Chinese with English abstract). *Acta Petrol Sin* 23:1217–1238
- Xi BB, Zhang DH, Zhou LM, Zhang WH, Wang C (2008) Characteristics of ore-forming fluid evolution in Dajishan tungsten deposit, Quannan county, Jiangxi (in Chinese with English abstract). *Acta Geol Sin* 82:956–966
- Xiao J, Wang Y, Hong YL, Zhou YZ, Xie MH, Wang DS, Guo JS (2009) Geochemistry characteristics of Xihuashan tungsten granite and its relationship to tungsten metallogenesis (in Chinese with English abstract). *J East China Inst Technol* 32:22–31
- Xie MH, Wang DS, Lu SM (2008) Prospecting potential of tungsten ore in southwest of Xihuashan in Jiangxi Province (in Chinese with English abstract). *J East China Inst Technol* 31:201–206
- Xie MH, Wang MJ, Shen H, Peng J, Chen RY (2009) Prelim probe on the geological characteristics and metallogenic law of continuous resource exploration area in Xihuashan tungsten deposit (in Chinese with English abstract). *J East China Inst Technol* 32:213–218
- Yan DP, Zhou MF, Song HL, Wang XW, Malpas J (2003) Origin and tectonic significance of a Mesozoic multi-layer over-thrust system within the Yangtze Block (South China). *Tectonophysics* 361:239–254
- Yokart B, Barr SM, Williams-Jones AE, Macdonald AS (2003) Late-stage alteration and tin-tungsten mineralization in the Khuntan Batholith, northern Thailand. *J Asian Earth Sci* 21:999–1018
- Yoo B, Lee H, White N (2010) Mineralogical, fluid inclusion, and stable isotope constraints on mechanisms of ore deposition at the Samgwang mine (Republic of Korea)—a mesothermal, vein-hosted gold-silver deposit. *Miner Depos* 45:161–187
- Zaw K, Peters SG, Cromie P, Burrett C, Hou Z (2007) Nature, diversity of deposit types and metallogenic relations of South China. *Ore Geol Rev* 31:3–47
- Zeng YS, Zhu YF, Liu JQ (2001) Carbonaceous material in S-type Xihuashan granite. *Geochem J* 35:145–154
- Zhang YG, Frantz JD (1987) Determination of the homogenization temperatures and densities of supercritical fluids in the system

- NaCl–KCl–CaCl₂–H₂O using synthetic fluid inclusions. *Chem Geol* 64:335–350
- Zhang LG, Zhuang LC, Qian YQ, Guo YS, Zhai P (1981) Stable isotope geochemistry of granites and tungsten-tin deposits in Xihuashan-Piaotang area, Jiangxi Province, China (in Chinese). *Proceedings of Symposium on Tungsten Geology*. Geological Publishing House, Beijing, pp 325–338
- Zhang LG, Liu JX, Chen ZS, Zhou HB (1994) Experimental investigations of oxygen isotope fractionation in cassiterite and wolframite. *Econ Geol* 89:150–157
- Zhao MQ, Lu ZM, Liu ZQ (1998) Circulation of ore-forming fluid in the filling of wolframite-bearing quartz veins in the tungsten deposit, Southern China (in Chinese with English abstract). *Geol Explor Non-ferrous Met* 7:272–276
- Zhou MF, Yan DP, Kennedy AK, Li YQ, Ding J (2002) SHRIMP U–Pb zircon geochronological and geochemical evidence for Neoproterozoic arc-magmatism along the western margin of the Yangtze Block, South China. *Earth Planet Sci Lett* 196:51–67
- Zhou YZ, Hong YL, Wu CJ, Han ZX, Wen LH (2008) On the utilization of tungsten resources of Xihuashan mine and its substitution resource prospecting (in Chinese with English abstract). *China Tungsten Ind* 23:13–17
- Zoheir B, Akawy A, Hassan I (2008) Role of fluid mixing and wallrock sulfidation in gold mineralization at the Semna mine area, central Eastern Desert of Egypt: evidence from hydrothermal alteration, fluid inclusions and stable isotope data. *Ore Geol Rev* 34:580–596